Transported PDF Modeling of Jet-in-Hot-Coflow Flames

De, Ashoke; Sarras, Gerasimos; Roekaerts, Dirk

DOI
10.1007/978-981-15-5667-8_17

Publication date
2021

Document Version
Final published version

Published in
Sustainable Development for Energy, Power, and Propulsion

Transported PDF Modeling of Jet-in-Hot-Coflow Flames

Ashoke De, Gerasimos Sarras, and Dirk Roekaerts

1 Background

The need to avoid pollutant emissions has resulted in the development of new combustion techniques. These techniques include high-temperature air combustion (HiTAC), flameless oxidation combustion (FLOX), and moderate and intense low-oxygen dilution (MILD) combustion which falls under the category of 'clean combustion techniques.' One of the features of MILD combustion is the high re-circulation ratio. The hot gas re-circulation serves the combustion process in two ways; first, it raises the reactant temperature, providing the heat needed for stable ignition. Secondly, it reduces the oxygen concentration of the mixture which reduces the flame temperature and the thermal NO_x emissions. Other features of the MILD combustion include flat temperature field, low turbulence fluctuations, smooth radiation flux, and barely visible and audible flame [1–8].

Dally et al. [9] of the Adelaide University designed a jet-in-hot-coflow burner and carried out experiments producing detailed profiles of major as well as minor species. The experiments performed on this burner provided a comprehensive database that has been used in the present study. Various numerical studies [10–18] have also been carried out using these databases to evaluate the performance of different turbulence and combustion models.

There have been various RANS-based modeling studies carried out in the context of the Adelaide burner, most notable among them being the ones carried out by

A. De (✉)
Department of Aerospace Engineering, Indian Institute of Technology Kanpur, Kanpur 208016, India
e-mail: ashoke@iitk.ac.in

G. Sarras · D. Roekaerts
Department of Process and Energy, Delft University of Technology, Leeghwaterstraat 44, 2628 CA Delft, The Netherlands

A. De et al. (eds.), *Sustainable Development for Energy, Power, and Propulsion*, Green Energy and Technology,
https://doi.org/10.1007/978-981-15-5667-8_17

Christo and Dally [10, 11]. The major finding was the fact that the SKE turbulence model with a modified dissipation constant ($C_{\varepsilon 1} = 1.6$) produces the best agreement with the experimental results. Other notable RANS-based modeling studies include the ones carried out by Frassoldati et al. [12], Mardani et al. [13, 14], and Aminian et al. [15]. All of these studies made use of the EDC combustion model in combination with DRM 22 [19], GRI 2.11 [20], and KEE-58 [21] chemical mechanisms to study the flame structure and the effects of molecular diffusion on flame characteristics in the MILD regime. Kim et al. [16] simulated the JHC flames using the conditional moment closure (CMC) with the primary goal of understanding the flame structure and NO formation in the MILD regime. Ihme et al. [17, 18] studied the JHC flames using LES with the flamelet/progress variable (FPV) approach. They considered the burner as a three-stream mixing problem by introducing an additional conserved scalar to identify flamelets of different mixture compositions and showed that the coflow mixture composition could only inadequately be represented by one mixture fraction.

From the above review, it is evident that a major problem while modeling these flames is the nonlinear interaction between fluid mixing and finite rate chemistry in the MILD regime. The transported probability density function (PDF) method is suited to handle this problem. It allows us to include the effects of turbulence–chemistry interaction in the Reynolds-averaged Navier–Stokes (RANS) framework [22].

The objective of this work is to explore the predictive capability of flamelet-generated manifold (FGM) chemistry [23] in a RANS/PDF framework. The FGM has been successfully applied to simulations of various combustion systems [23–27]. In all these cases, a mixture fraction and a progress variable were adequate to create the table. This study is the first attempt to extend the FGM with a second mixture fraction to account for coflow inhomogeneity and air entrainment in predicting JHC flames in the MILD combustion regime. The numerical predictions obtained using this model are compared with experimental databases.

2 Tabulated Chemistry Construction[1]

2.1 Coflow Representation

In the following, the tabulated chemistry model is presented for describing a three-mixing problem. The chemistry data have been tabulated using the FGM approach. The FGM is based on laminar diffusion flamelets between the fuel ($CH_4 + H_2$) and the coflow (a mixture of combustion products and air). Since the coflow composition and temperature vary in space (Fig. 1), flamelets with different coflow compositions and temperatures are required. The mean temperature and mass fractions have

[1]This section is reproduced from Sarras et al. [27].

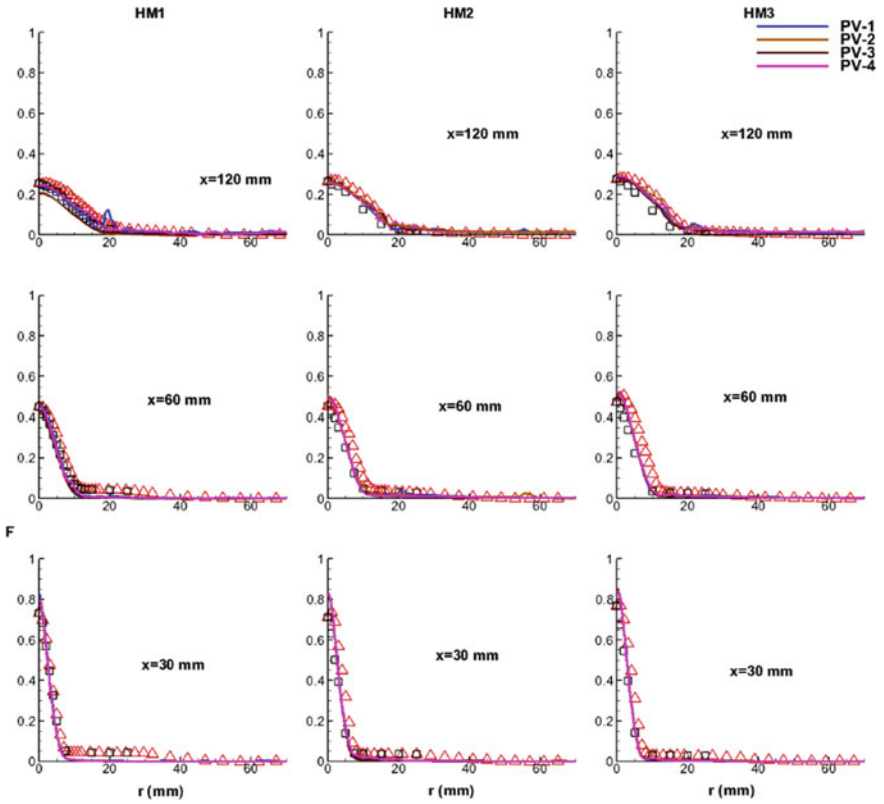

Fig. 1 Radial profiles of mean mixture fraction (F) using different PVs: (triangle $0 \leq r \leq 70$ and squares $-25 \leq r \leq 0$) symbols are measurements and lines are predictions

been measured along the radial direction of the coflow at $x = 4$ mm above the jet nozzle as shown in Fig. 1. Following the approach of Ihme and See [17], a second mixture fraction Z_2 is introduced, which will quantify the mixing between a coflow representative and the surrounding air and, at the same time, can be used to describe the variation in the coflow composition based on oxygen concentration. The coflow representative is defined at the radial position $r = r_{\text{rep}}$ such that:

$Y_{O_2}(r_{\text{rep}}) = \min(Y_{O_2}(r))$. For every point in the radial direction, we define:

$$Z_2(r) = \frac{Y_{O_2}(r) - Y_{O_2}(r_{\text{rep}})}{Y_{O_2}(r_{\text{air}}) - Y_{O_2}(r_{\text{rep}})} \tag{1}$$

The coflow representative is given by $Z_2 = 0$, and the cold ambient air is provided by $Z_2 = 1$. In this approach, the enthalpy deficit (Δh) relative to the adiabatic mixing is assumed strictly correlated with Z_2. To take into account that the enthalpy deficit is not a unique function of Z_2 and to allow independent fluctuations of Z_2 and Δh,

it would be necessary to consider Δh as an extra independent variable. Assuming chemical equilibrium at the coflow inlet, the full composition is entirely determined from Z_2. With this definition, the composition and temperature at the coflow inlet are functions of Z_2

$$\begin{aligned} Y_i(r) &= Y_i(Z_2(r)), \\ T(r) &= T(Z_2(r)). \end{aligned} \tag{2}$$

2.2 3D Manifold Construction

The FGM method is based on laminar flamelets. A flamelet is the solution of a low Mach number formulation of the one-dimensional Navier–Stokes equations supplemented with species and enthalpy equations, including detailed chemistry. The detailed chemistry model presently employed is the GRI 3.0 [20] reaction mechanism. Since the auto-ignition is the primary stabilization mechanism for the JHC [10] flames, unsteady effects should be included. Non-premixed unsteady laminar flamelets are formulated and solved in physical space and time with the CHEM1D code [28, 29]. Preferential diffusion effects are included using the mixture average approach. The initial condition for the unsteady flamelet solution is given by a pure mixing solution of the above boundary value problem. The oxidizer composition is a function of the second mixture fraction $Y_i^{\text{ox}} = (1 - Z_2)Y_i^{\text{rep}} + Z_2 Y_i^{\text{air}}$.

FGM tables have been constructed for a set of values of the second mixture fraction with corresponding enthalpy deficit levels. First, the values for the second mixture fraction have been chosen which correspond to a particular radial location, and these values are needed to represent accurately the enthalpy deficit range of the coflow. For each Z_2 value, a FGM table is constructed from a non-premixed igniting flamelet between fuel and the coflow composition at Z_2 with the corresponding enthalpy deficit, according to Fig. 1. A moderate strain rate $a = 100\,\text{s}^{-1}$ is used in all the flamelet calculations. For each of the coflow compositions, the solution is stored at successive time instances. These solution files form the base of the 2D-FGM construction. A total of ten 2D-FGMs are obtained.

The first step in the 2D-FGM construction consists of defining a suitable progress variable Y. In any given flamelet (i.e., fixed Z_2 value), the progress variable must be a monotonic function of time at each physical position. Since the first mixture fraction is a monotonically increasing function of the spatial coordinate [25], this requirement can also be stated in terms of the first mixture fraction instead of the spatial position. The reaction progress variable in this work is defined by

$$Y = \sum_i \frac{Y_i}{M_i}, \tag{3}$$

where Y_i is the mass fraction of CO_2, CO, H_2, H_2O, or CH_4 and M_i denotes the molar mass of the considered species. Then, the 2D-FGM is simply obtained by transforming the dependence on the spatial coordinate into a dependence on the first mixture fraction and time into dependence on the reaction progress variable

$$\phi(x, t; Z_2) \rightarrow \phi_{\mathrm{FGM}}(Z_1, Y; Z_2) \tag{4}$$

where ϕ stands for any thermochemical variable. In practice, this transformation is obtained by sorting and relabeling the data in each flamelet such that all dependent variables are stored as a function of the mixture fraction Z_1 and the scaled progress variable c. The scaled progress variable is defined by

$$c = \frac{Y - Y_{\min}(Z_1)}{Y_{\max}(Z_1) - Y_{\min}(Z_1)}, \quad c \in [0, 1] \tag{5}$$

The minimum $Y_{\min}$ and maximum $Y_{\max}$ values of the unscaled progress variable are also stored.

The 3D-FGM is obtained by combining the 10 different 2D-FGMs. Then, every local thermochemical state can be described by using the three independent variables Z_1, Z_2, Y,

$$\phi = \phi(Z_1, Y; Z_2). \tag{6}$$

The computer program FLAME [30] developed at the TU Delft has been used to optimize the tabulation of the 3D-FGM. In the FLAME code, the physical range of the four independent variables is mapped onto a cube $[0, 1]^3$ to facilitate adaptive grid refinement. The grid refinement automatically detects regions in composition space (Z_1, Z_2, Y) with large gradients of the dependent variables and inserts grid points as necessary to resolve the gradients. The adaptive tabulation uses linear interpolation between any two 2D-FGMs (Z_2 direction) and within each 2D-FGM ($Z_1 - Y$ plane). For consistency, the density is not interpolated but is recalculated based on the interpolated temperature and composition. In addition to the relevant thermochemical variables, the source term of the progress variable is stored in the table,

$$S_Y(Z_1, Z_2, Y) = \frac{\dot{\omega}_Y}{\rho}. \tag{7}$$

However, special care has to be taken for the source term at the boundary $Y = Y_{\max}(Z_1, Z_2)$ which corresponds to the steady-state flamelet solution. In the steady state, we have

$$\frac{\partial \rho u Y_{\max}}{\partial t} - \frac{\partial}{\partial x}\left(\frac{\lambda}{c_p}\frac{\partial \rho Y_{\max}}{\partial x}\right) + \rho G Y_{\max} - \rho S_{Y_{\max}} = 0 \tag{8}$$

and hence, in general $S_{Y_{\max}} \neq 0$. Without any further measures, this leads to the occurrence of $Y > Y_{\max}(Z_1, Z_2)$. To avoid this problem, we set $S_{Y_{\max}} = 0$ which holds in chemical equilibrium as obtained in a steady flamelet with a strain rate $a \to 0$.

3 PDF Formulation with 3D-FGM Table

The details of the in-house PDFD code and the PDF method can be found in Refs. [31–33]. Here, we only describe the modifications that have been made to use the 3D-FGM in the PDFD simulations. Every Monte Carlo particle carries two mixture fractions Z_1, Z_2 and a reaction progress variable Y. This means that every particle now evolves in composition space according to the general equation:

$$\mathrm{d}\phi_\alpha^* = \theta_{\alpha,\mathrm{mix}}^* \mathrm{d}t + S_\alpha\left(\vec{\phi}\right)\mathrm{d}t \tag{9}$$

where $\vec{\phi} \equiv (Z_1, Z_2, Y)$ and $\alpha = 1, 2, 3$. Also, $\theta_{\alpha,mix}$ represents the chosen micro-mixing model and $S_\alpha\left(\vec{\phi}\right)$ the chemical source term of the progress variable. The mixture fractions are not affected by chemical reactions, and their values only change according to the chosen micro-mixing model. Radiative heat losses are not included here. The evolution of the reaction progress variable is split into a micro-mixing step and a reaction step. Micro-mixing is performed first, and then the reaction step is mainly based on an explicit Euler scheme:

$$\mathrm{d}Y = S_Y(\phi) \cdot \mathrm{d}t \tag{10}$$

where S_Y is the source term and t is the time step. A Runge–Kutta method [32] is implemented to accurately advance the progress variable changes due to the highly nonlinear source terms. In all the igniting flamelets, the source term is a very smooth function of the progress variable, and hence the gradients are small. The boundary conditions for the reaction progress variable at any radial position at the inlet are given by

$$Y = Y_{\min}(0, Z_2(r) = \mathrm{const}) \tag{11}$$

The local composition is given by the two mixture fractions and the reaction progress variable. All other scalar variables (temperature, species mass fractions, density, etc.) are retrieved from the lookup table.

4 Simulation Details

A detailed description of the burner geometry can be referred from Dally et al. [9, 10]. In the context of the numerical setup, a very similar numerical setup, explained above, with a few changes has been used to model the methane–hydrogen JHC flames in the Adelaide burner. Three different flames with different oxygen contents in the hot coflow have been simulated, namely HM1 (3% O_2), HM2 (6% O_2), and HM3 (9% O_2). The Reynolds number has been kept constant at Re = 10,000 for all three flames.

A 2D axisymmetric grid has been used in the simulations. As the central fuel jet protrudes 4 mm at the jet exit, the computational domain starts 4 mm downstream of the jet exit and extends for 300 mm in the axial direction and 80 mm in the radial direction. The grid consists of 200 × 120 cells in the axial and radial direction, respectively (stretched in both directions). At the end of the computational domain, in the axial direction, the boundary condition is set to outflow. For the fuel jet inlet, the velocity profiles are used from a detailed separate simulation, whereas at the hot and cold coflow inlets, the velocity boundary conditions are set to 3.2 m/s and 3.3 m/s, respectively. As per the previous studies, the solution is very sensitive to the turbulent quantities at the inlet; therefore, the turbulent intensities at the hot and cold coflow have been set to 5%, while it is set to 7% at the fuel jet inlet as per the published results [8, 12].

The flamelet-generated manifold for the methane–hydrogen combustion is based on the GRI 3.0 [20] chemical mechanism with 53 species and 325 chemical reactions. The radial profiles of the temperature and species mass fraction with experimental values at $x = 4$ mm have been used to create the FGM tables. The FGM table resolution is set to $Z \times Y = 201 \times 201$ points with equidistant spacing.

The PDF transport equation was solved using the Lagrangian Monte Carlo approach initialized with approximately 20 particles per cell. The effect of micro-mixing models is also studied with a mixing constant $C_\phi = 2$. The Reynolds number has been kept constant at Re = 10,000. The results obtained are compared with the respective experimental database, and the profiles of mean temperature, mean mixture fraction, and major species are reported.

5 Results and Assessment[2]

In this section, the simulation results are presented for three flames, i.e., HM1, HM2, and HM3. The profiles of mean temperature, mean mixture fraction, and major species are reported and are compared with the respective experimental database.

[2]Some portion of this section is reproduced from De et al. [8].

5.1 *Effect of Progress Variable*

Initially, we have considered a different linear combination of PV to test the sensitivity of the PV in predictions. The mixing model is kept constant for all the simulation, and that is IEM. The considered combination is defined as:

$$\mathrm{PV1} = \mathrm{CO_2} + \mathrm{H_2O} + \mathrm{H_2}$$

$$\mathrm{PV2} = \mathrm{CO} + \mathrm{CO_2} + \mathrm{H_2O}$$

$$\mathrm{PV3} = \mathrm{CO} + \mathrm{CO_2} + \mathrm{H_2O} + \mathrm{H_2}$$

$$\mathrm{PV4} = \mathrm{CO} + \mathrm{CO_2} + \mathrm{H_2O} + \mathrm{H_2} + \mathrm{CH_4}$$

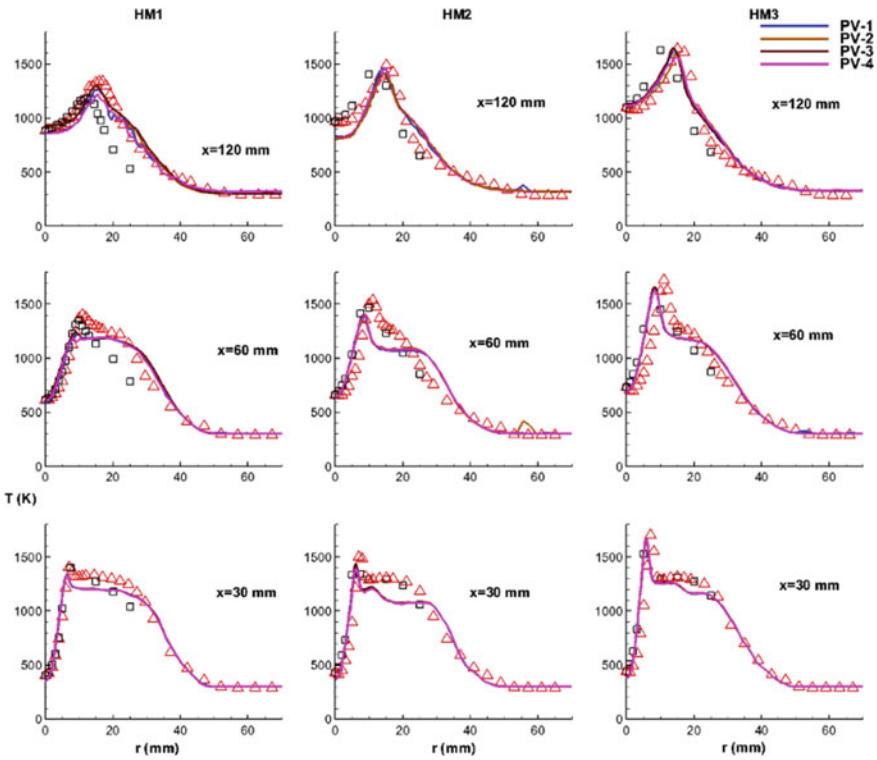

Fig. 2 Radial profiles of mean temperature using different PVs: Symbols are measurements and lines are predictions (legends are the same as Fig. 1)

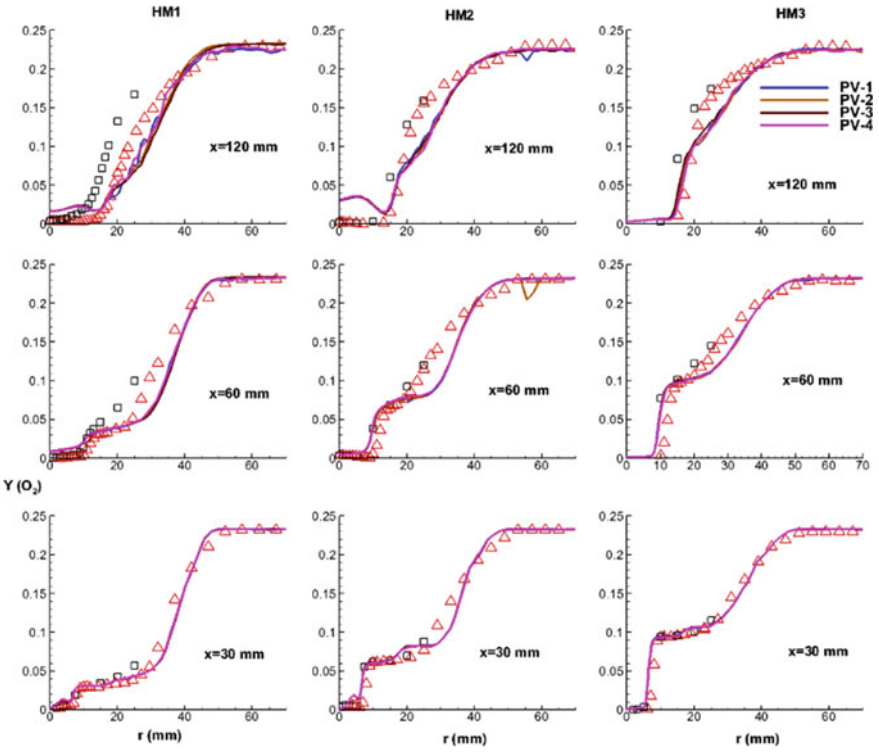

Fig. 3 Radial profiles of mean O_2 using different PVs: Symbols are measurements and lines are predictions (legends are the same as Fig. 1)

Figures 1, 2, and 3 depict the radial profiles of mean mixture fraction, temperature, and one major species (O_2) using different PVs. As observed from the figures, the predictions are not sensitive to the different combinations of PV, thereby not showing any significant differences in results.

This means the linear combination of major species is good enough for the predictions of these flames. Hence, the rest of the results are reported with PV3 only, which is precisely the same as reported in the published work by Ihme et al. [18] to make an assessment of our predictions.

5.2 Effect of Mixing Models and PDF Models

In this section, using the PV3 definition, a detailed analysis is carried out. Two critical parameters are varied here are: (a) mixing models: IEM, CD, EMST, and (b) PDF models: scalar composition PDF and joint velocity-scalar composition PDF.

Figure 4 shows the profiles of the mean mixture fraction obtained for HM1 flame. As observed, all the models capture the profiles accurately, and no significant differences are observed among these predictions except the CD model. Some discrepancies can be observed in the mean temperature profiles as depicted in Fig. 4. The predictions are similar for HM2 and HM3 flames. For HM1 flame, the centerline temperature profiles are overpredicted; however, the predictions are improved along with the shear layer. Among the transported PDF models, the LPDF-EMST predictions are better compared to the LPDF-IEM and LPDF-CD predictions, especially for HM1 flame. No significant differences are observed using only the scalar composition PDF method, as represented using '*Sc*' in all the plots. The peak temperature predictions are reasonably well, while some discrepancies are observed at the outer shear layer, especially the case with lower O_2 concentration, i.e., HM1 flame. Even though the LPDF-CD predictions are consistently poor in all three flames, we can observe an improvement in the predictions as the oxygen content in the coflow increases. As the oxygen content in the hot coflow increases from 3% (by mass) in HM1 to 6% in HM2 and to 9% in HM3 flames, the reaction rate improves due to which the models are able to predict the flames with better accuracy and a clear improvement in the temperature predictions, obtained using all the models.

Figure 5 depicts the profiles of mean CH_4 and H_2 mass fraction obtained for HM1 flame. Near the jet exit, the peak of CH_4 is overpredicted by all the models, but the mean H_2 profiles are found to be good. Major discrepancies can be observed in O_2 predictions for all three flames, as shown in Figs. 6, 7, and 8. In this case, the dominance of scalar composition PDF is observed at the downstream locations. Even after providing better boundary conditions for oxygen (obtained from $x = 4$ mm measurements) for all three flames, the evolution of O_2 could not be captured accurately. This discrepancy is primarily due to the handling of reaction rate in modeling (turbulence–chemistry interaction) and cannot be quantified unless we look at the velocity statistics in the domain, and this remains another drawback of this burner as it does not provide any velocity data. Among the LPDF models, there are no substantial differences observed between IEM and EMST predictions for all three flames, but as we move to HM2 and HM3, we observe the predictions appear to be in better shape, especially, for HM3 flame. For all three flames, LPDF-CD predictions show substantial differences from the other two models [8].

The profiles of mean CO_2 and H_2O mass fraction obtained for HM1, HM2, and HM3 flames are shown in Figs. 9, 10, and 11. All the models adequately capture the profiles near the jet exit area, but the centerline profiles are consistently overpredicted. Discrepancies can be observed for the predictions away from the jet exit at $x = 120$ mm location. The profiles of mean H_2O mass fraction exhibit a completely different picture from that of CO_2 profiles. As the oxygen content increases in the coflow from HM1 to HM3 flames, the extent of under-prediction at the centerline also increases. Previous studies all reported similar behavior where they have looked at the impact of chemical kinetics; however, the present study includes fairly detailed chemistry. Thus, we can assert that the chemical mechanism is not primarily responsible for the predictions obtained herein. However, it should be noted that the turbulent timescale is the dominant factor along the centerline, which supersedes the scalar

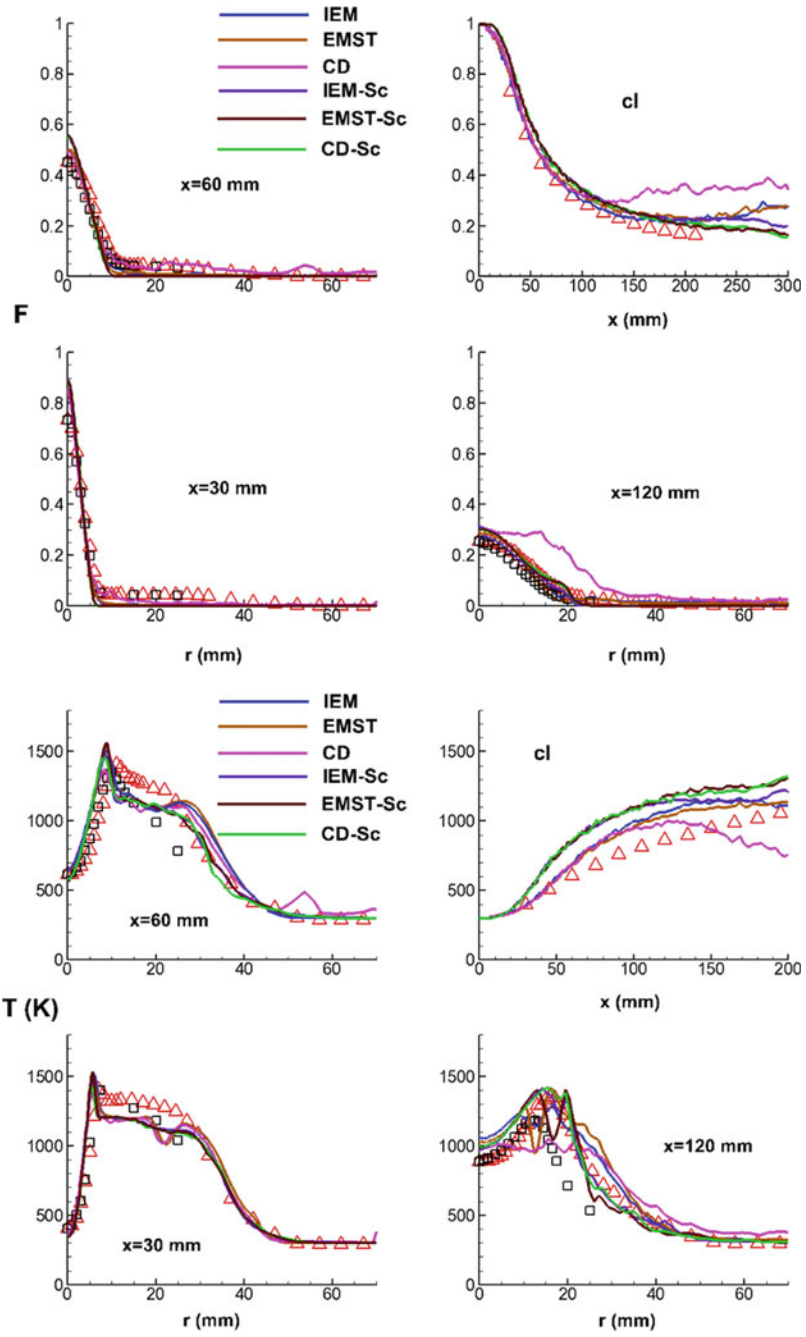

Fig. 4 Profiles of mean mixture fraction and temperature for HM1 flame (legends are the same as Fig. 1). '*Sc*' stands for scalar composition PDF

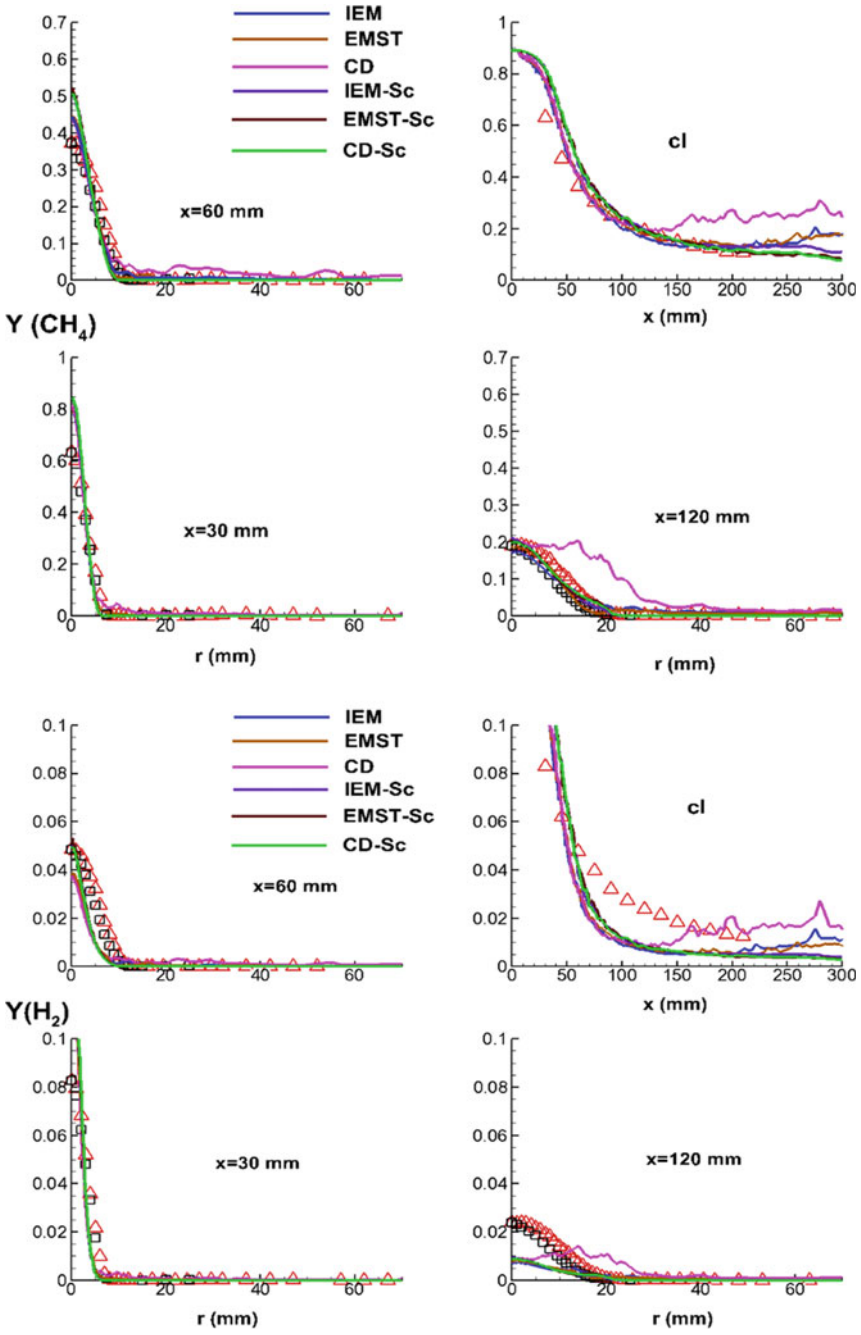

Fig. 5 Profiles of mean CH_4 and H_2 for HM1 flame (legends are the same as Fig. 1)

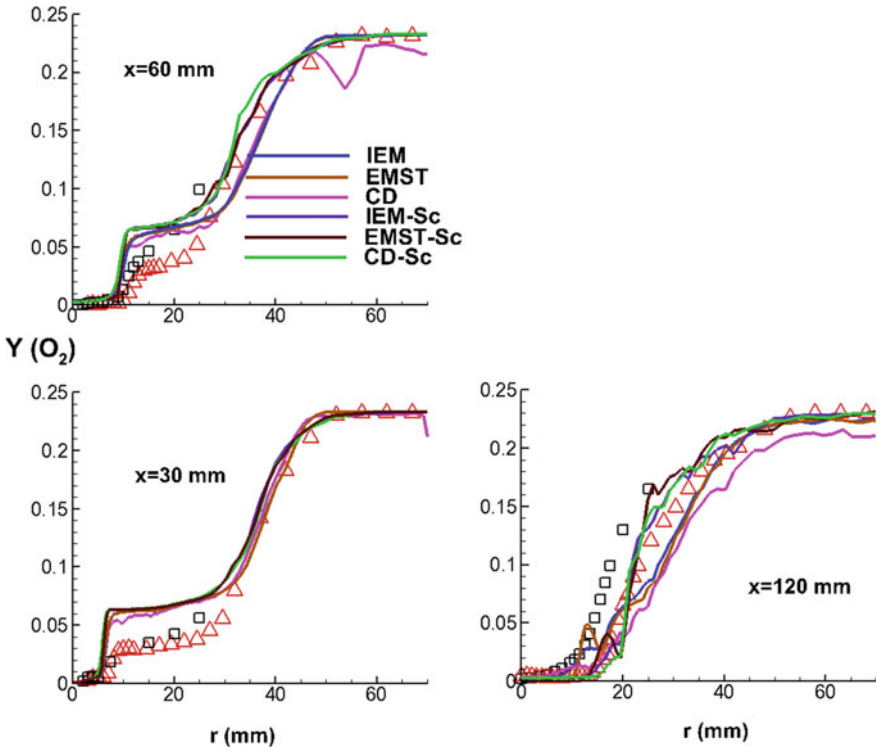

Fig. 6 Profiles of mean O_2 for HM1 flame (legends are the same as Fig. 1)

dissipation timescale, and hence the combustible mixture dissipates quickly as the species are not allowed to stay for a longer duration in this region to complete reaction. This is one of the major reasons behind the discrepancies observed in species profiles along the centerline, especially the O_2 profiles and temperature, in turn, affecting the CO and H_2O profiles. This slow chemistry increases the chemical timescales and, in turn, reduces the Damkohler number, and all the combustion models are unable to capture the flame characteristics in this low Damkohler number range, which has significantly affected the species predictions.

To better understand the model behavior, it is worthwhile to look at the predictions of minor species like OH and CO. Major discrepancies can be observed in Figs. 12, 13, and 14 depicting OH and CO profiles, respectively. Looking at the radial profiles of OH obtained for HM2 and HM3 flames, it can be seen here that the predictions are in better shape compared to those obtained for HM1 flame as the oxidation of O_2 into OH is sufficiently captured. The CO profiles are significantly under-predicted in the shear layer between fuel jet and hot coflow for HM2 and HM3 flames. The CO profiles are better in HM3 compared to those obtained in the HM2 flame owing to the better performance of combustion models due to improved reaction rates and oxygen contents in the coflow. While comparing all the models, it has been observed that the

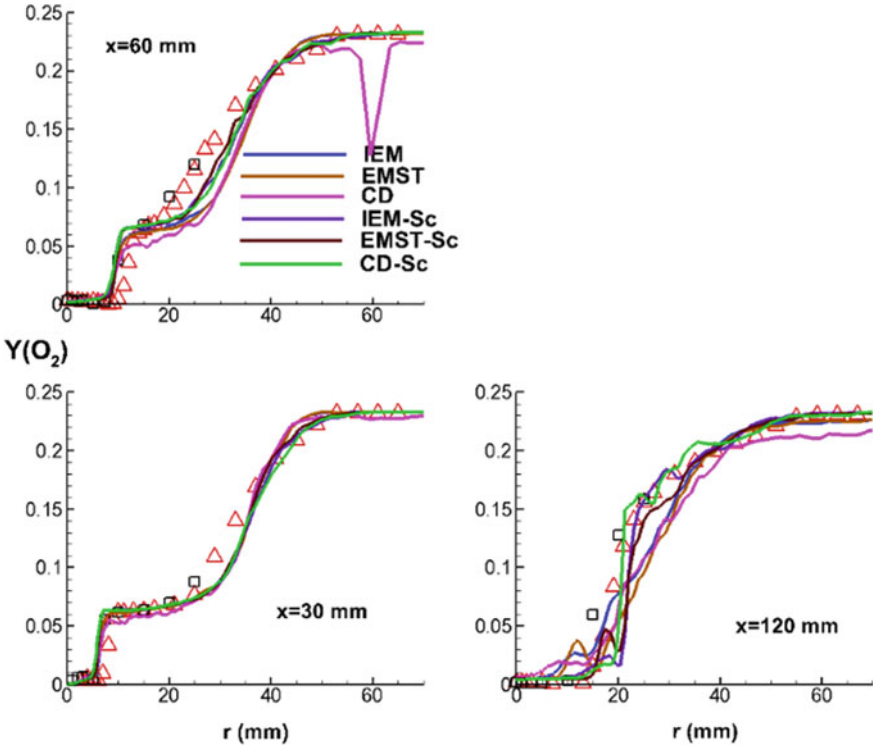

Fig. 7 Profiles of mean O_2 for HM2 flame (legends are the same as Fig. 1)

differences between EMST and IEM predictions are small and better compared to the CD predictions, which show considerable deviation from the two. It can be noted that the CO → CO_2 conversion is significantly affecting the proper predictions of CO_2, whereas OH → H_2O conversion is not significantly affecting the H_2O predictions. These phenomena are strongly coupled between turbulence–chemistry interaction models and chemical mechanism which needs further investigation [8].

The discrepancies observed, so far, with the finite rate chemistry-based models arise due to multiple reasons. Slower reaction rates in JHC flames, compared to standard combustion processes, make it more challenging for modeling. Despite having the chemical source terms in closed form, the transported PDF models cannot also be precisely accurate as the major source of errors in these models comes from the inaccuracies of the micro-mixing closures. The predictions in the shear layer are primarily affected due to mixing between the hot coflow and the fuel jet. This mixing between the streams, due to turbulence and species gradients, emphasizes the role of micro-mixing here. In case of IEM model [34], the composition of all the scalars relaxes toward the mean composition at the same rate whereas in case of CD mixing model, a number of particles in a cell are randomly selected and their individual compositions are moved toward the mean composition [35]. Therefore,

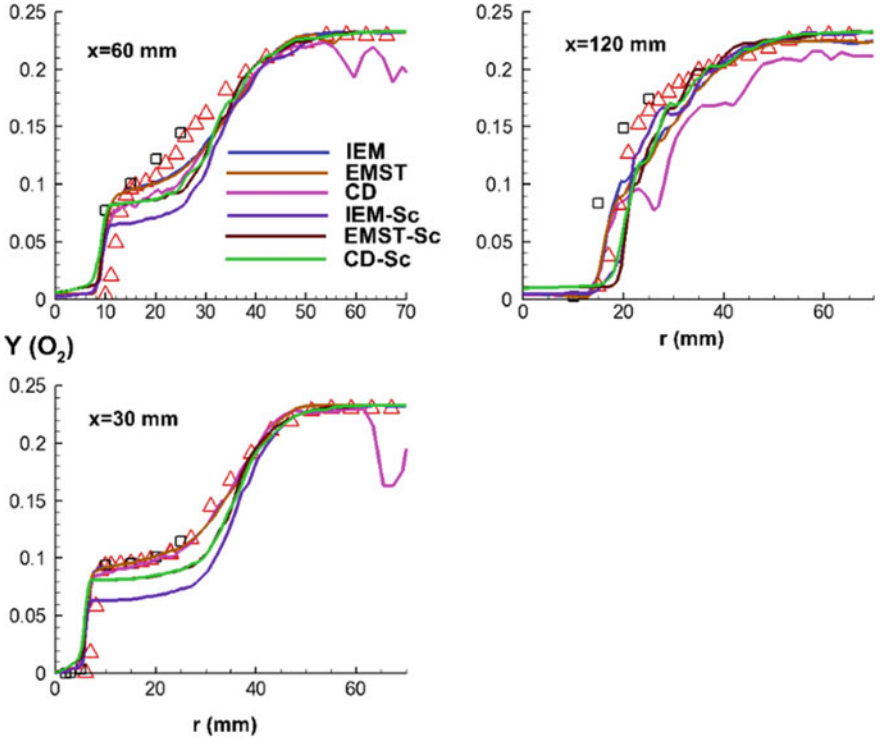

Fig. 8 Profiles of mean O_2 for HM3 flame (legends are the same as Fig. 1)

both of these mixing models are missing the effect of localness in the flow field which is a potential source of errors for the discrepancies observed in the predictions obtained through these models. However, on the contrary, the EMST model [36] takes into account the effects of local mixing among the particles in the composition space, thereby making it more accurate compared to the CD and the IEM models. Since, in the case of the CD mixing model, the particles, in a cell, are selected randomly, CD formulation is missing the effects of localness in the composition space, which is the main reason behind the differences observed between EMST and CD predictions. Another potential source of errors may arise from the 'notional particles' used in Lagrangian PDF approach: one due to particle tracking scheme and another one due to Monte Carlo methods. The mean density of particles in physical space should remain proportional to the local mean fluid density all the times, and this can be satisfied as long as the particle systems evolve consistently with the Eulerian equation systems. Therefore, the accuracy of the particle tracking scheme may induce some errors. The second source of discrepancies in the LPDF predictions is the numerical errors associated with the Monte Carlo methods, e.g., statistical errors and bias errors. Statistical errors are the random errors, whereas bias errors are deterministic errors, and both of them are strongly dependent on the

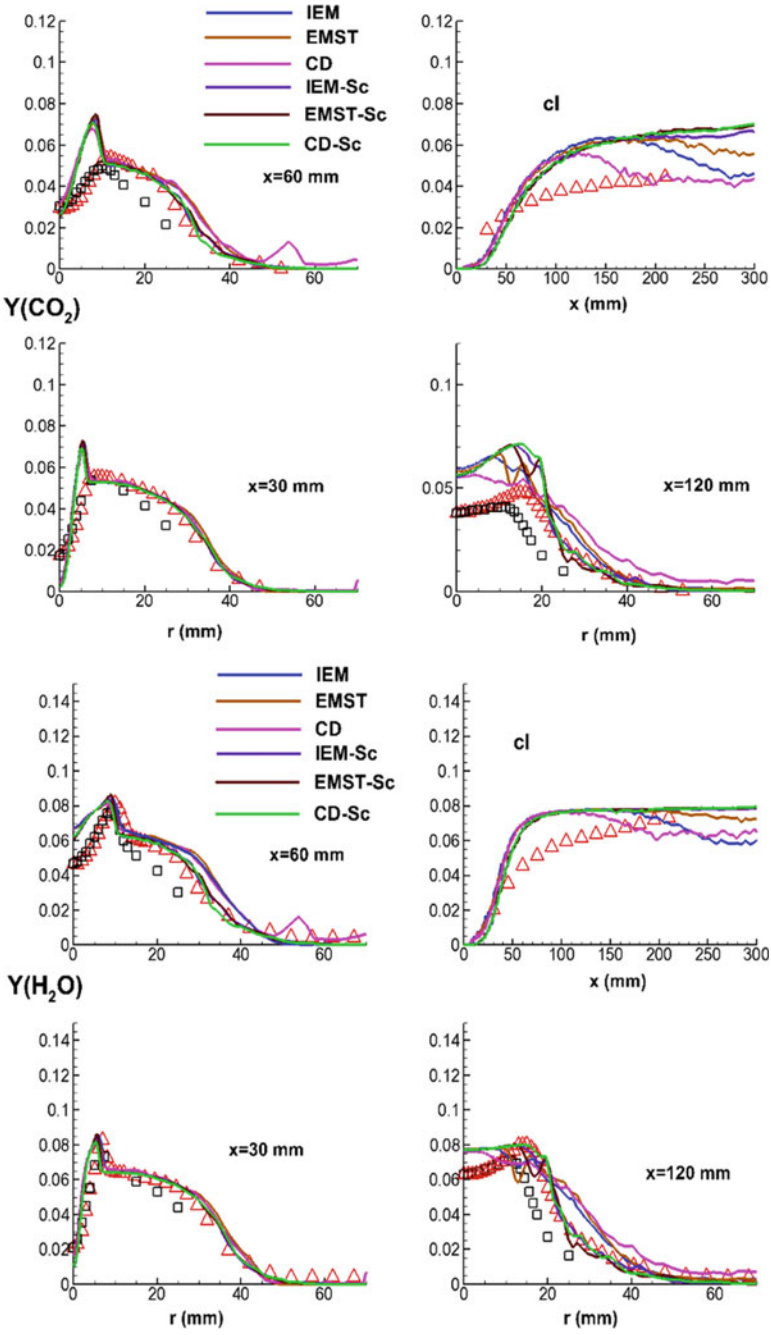

Fig. 9 Profiles of mean CO_2 and H_2O for HM1 flame (legends are the same as Fig. 1)

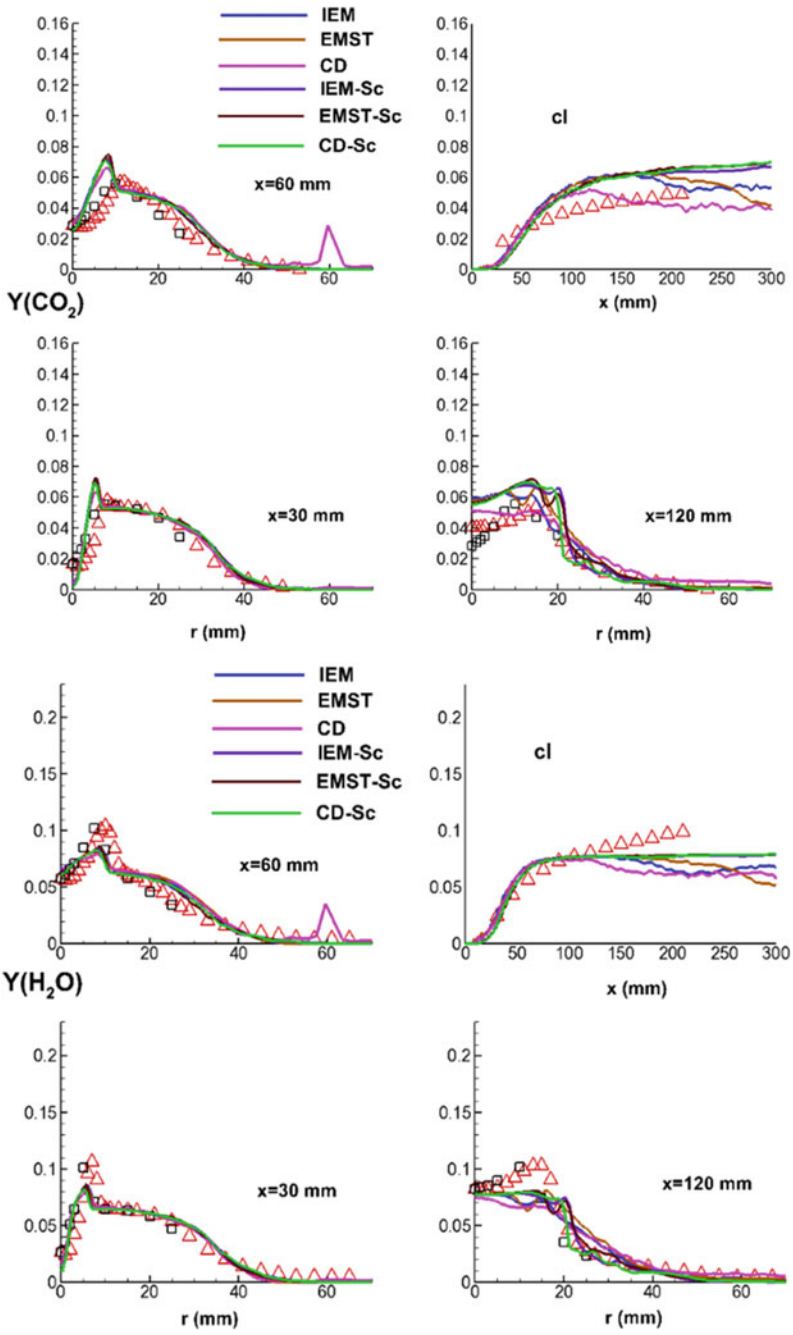

Fig. 10 Profiles of mean CO_2 and H_2O for HM2 flame (legends are the same as Fig. 1)

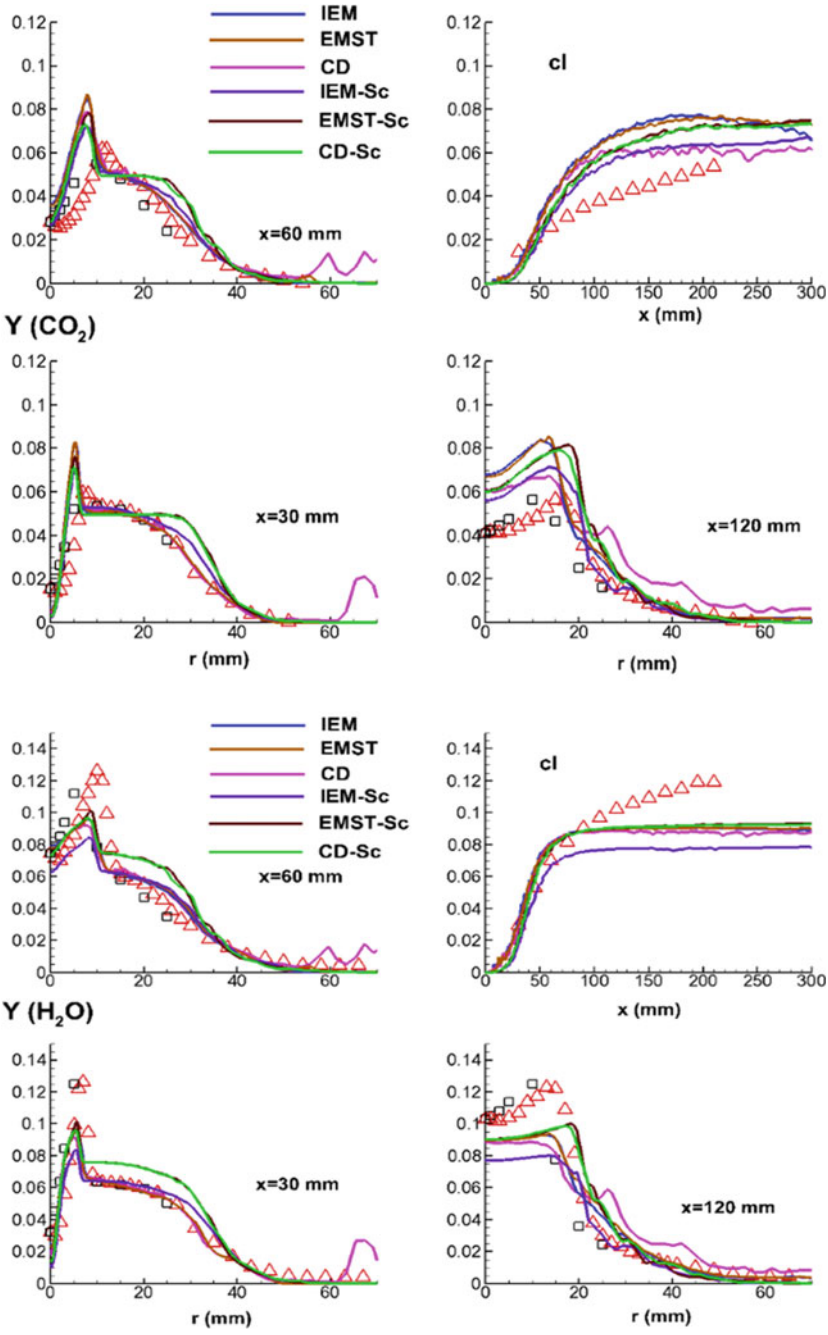

Fig. 11 Profiles of mean CO_2 and H_2O for HM3 flame (legends are the same as Fig. 1)

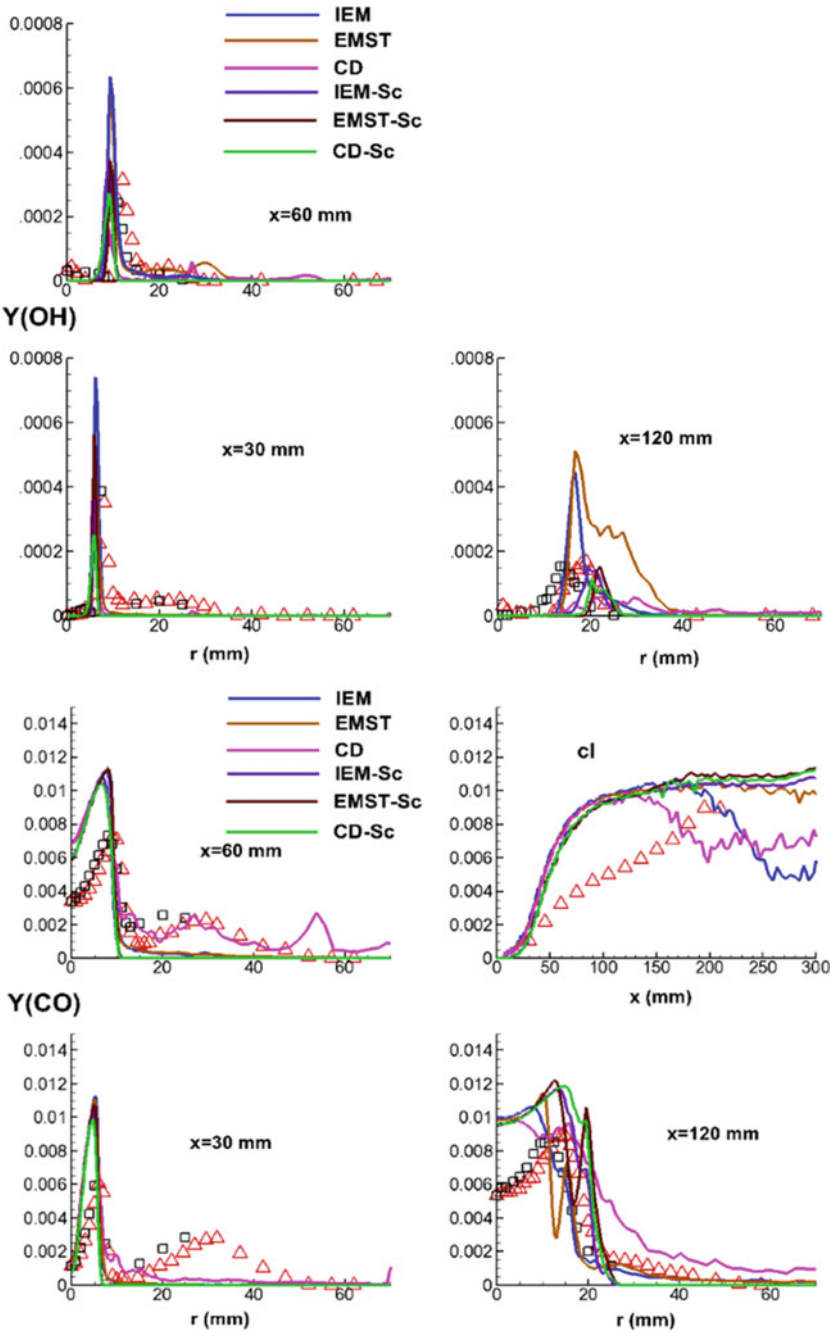

Fig. 12 Profiles of mean OH and CO for HM1 flame (legends are the same as Fig. 1)

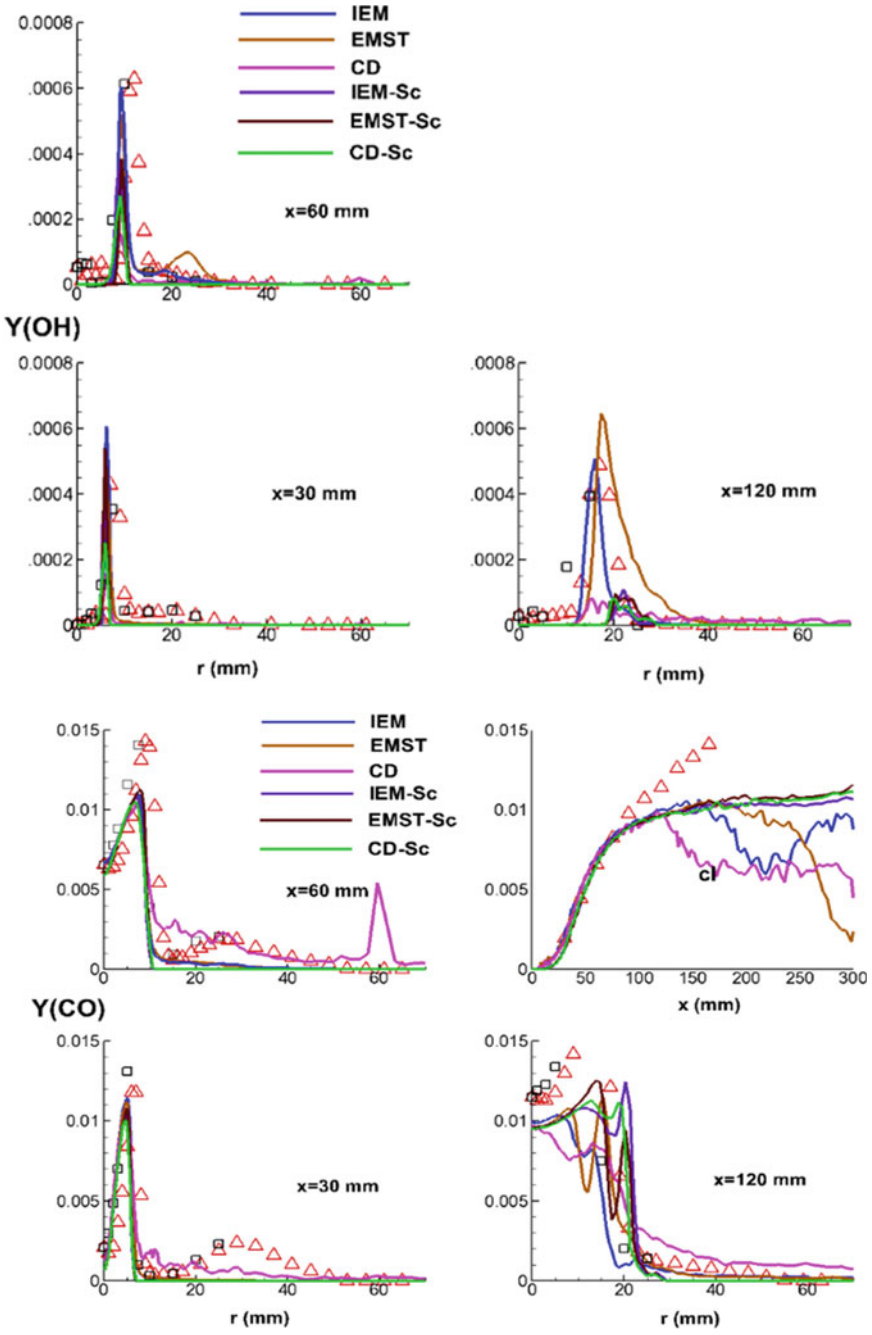

Fig. 13 Profiles of mean OH and CO for HM2 flame (legends are the same as Fig. 1)

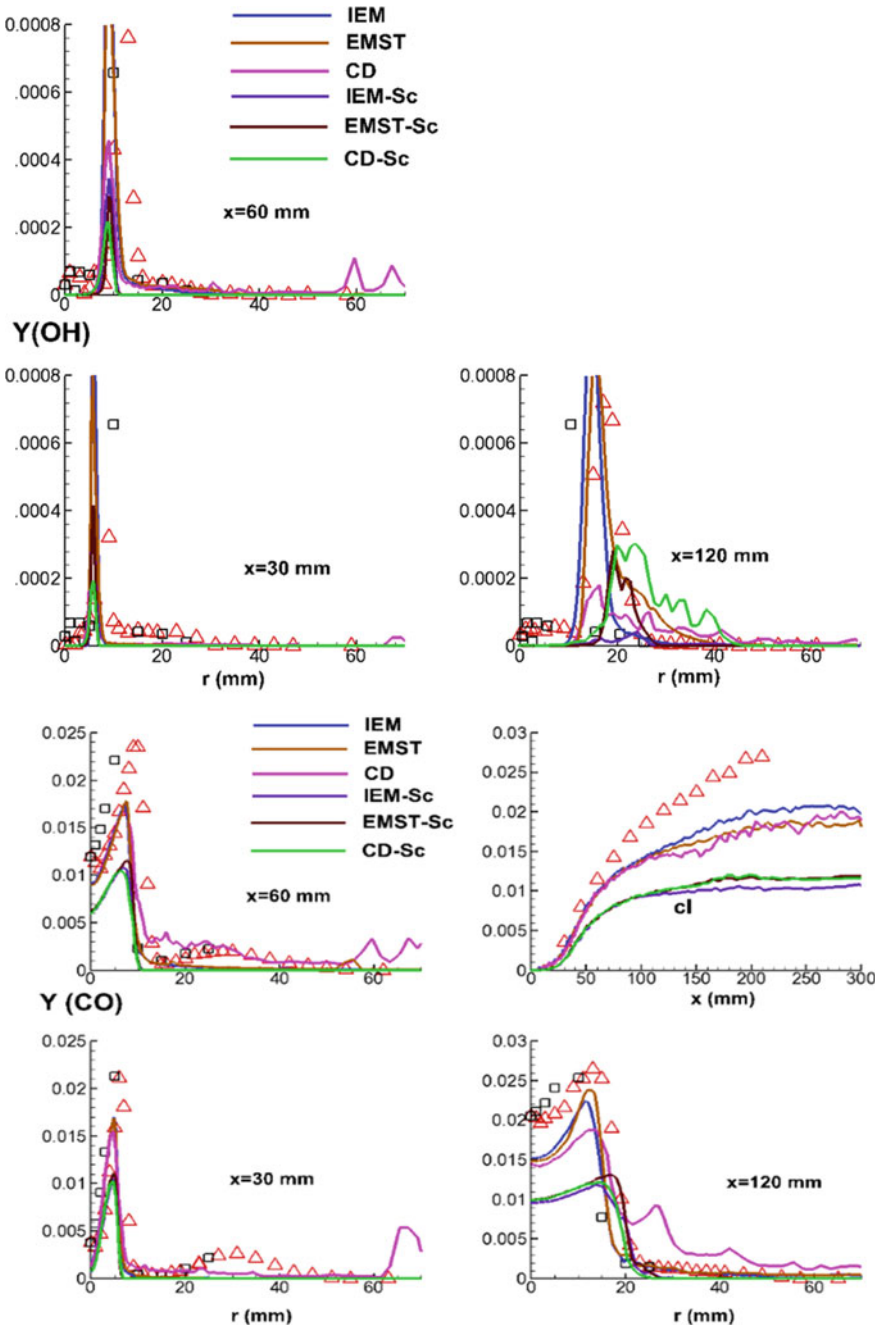

Fig. 14 Profiles of mean OH and CO for HM3 flame (legends are the same as Fig. 1)

number of particles used per cell. Statistical errors are not present in the present simulations; however, the bias errors, which arise from the mean quantities, are not completely reduced by averaging [8, 21].

In the JHC flames, the initiation of reaction is delayed, and overall reaction rates are lower than the conventional flames with lower temperatures and NO_x emissions. For the HM1 flame, there is 3% oxygen in the coflow, which is too much dilution for a JHC flame, and hence the HM1 flame forms a very crude case for studying the combustion models. Thus, comparing all the flames spread over a wide range of $O_{2\%}$ (3–9) at the end, it is evident that predictions improve as the oxygen content of the coflow increases, the reaction rate also increases, which, in turn, increases the Damkohler number. Therefore, we can say that we obtain better results at high Damkohler numbers irrespective of the chosen turbulence–chemistry interaction models. Overall, the mean predictions obtained through transported PDF-based models are in good agreement with some discrepancies observed mostly in the shear layer between the fuel jet and the hot coflow.

6 Conclusion

The performance of hybrid RANS/PDF method including tabulated chemical kinetics to predict the JHC flames is reported. A 3D-FGM table based on two mixture fractions and a reaction progress variable has been constructed to account for the inhomogeneity of the coflow and the entrainment of the ambient air. Igniting counterflow diffusion flamelets are created for different coflow compositions quantified by the second mixture fraction. To assess the predictive capability of the 3D tabulated chemistry manifold, Adelaide JHC flames have been considered for varying degrees of parameters. Comparison between predicted measurements is found to be in good agreement. It can be inferred from the present simulations that the 3D-FGM-based tabulated chemistry has the potential to predict JHC flame combustion with greater accuracy, and the sensitivity of current methodology needs further investigation for betterment.

Acknowledgements The first author would like to thank the Science and Engineering Research Board (SERB), India, for providing financial support. Further, the first author would also like to acknowledge the IITK Computer Center (www.iitk.ac.in/cc) for providing support to perform the computation work, data analysis, and article preparation.

References

1. Oldenhof E, Tummers M, van Veen EH, Roekaerts DJEM (2010) Ignition kernel formation and lift-off behavior of jet-in-hot-coflow flames. Combust Flame 157:1167–1178
2. Oldenhof E, Tummers MJ, van Veen EH, Roekaerts DJEM (2010) Role of entrainment in the stabilization of jet-in-hot-coflow flames. Combust Flame 157(6):1167–1178

3. Oldenhof E, Tummers MJ, van Veen EH, Roekaerts DJEM (2012) Transient response of the Delft jet-in-hot coflow flames. Combust Flame 159(2):697–706
4. De A, Oldenhof E, Sathiah P, Roekaerts D (2011) Numerical simulation of Delft-Jet-in-Hot-Coflow (DJHC) flames using Eddy Dissipation Concept (EDC) model for turbulence-chemistry interaction. Flow Turbul Combust 87(4):537–567
5. De A, Dongre A, Yadav R (2013) Numerical investigation of Delft-Jet-in-Hot-Coflow (DJHC) burner using Probability Density Function (PDF) transport modelling. In: ASME Turbo Expo, San Antonio, TX, 2012, ASME paper GT2013-95390
6. Bhaya R, De A, Yadav R (2014) Large Eddy Simulation of MILD combustion using PDF based turbulence-chemistry interaction models. Combust Sci Technol 186:1138–1165
7. Dongre A, De A, Yadav R (2014) Numerical investigation of MILD combustion using multi-environment Eulerian probability density function modeling. Int J Spray Combust Dyn 6(4):357–386
8. De A, Dongre A (2015) Assessment of turbulence-chemistry interaction models in MILD combustion regime. Flow Turbul Combust 94:439–478
9. Dally BB, Karpetis AN, Barlow RS (2002) Structure of turbulent non-premixed jet flames in a diluted hot coflow. Proc Combust Inst 29:1147–1154
10. Christo FC, Dally BB (2005) Modeling turbulent reacting jets issuing into a hot and diluted coflow. Combust Flame 142(1–2):117–129
11. Christo FC, Dally BB (2004) Application of transport PDF approach for modeling MILD combustion. In: 15th Australasian fluid mechanics conference, Sydney, Australia, 13–17 Dec
12. Frassoldati AF, Sharma P, Cuoci A, Faravelli T, Rangi E (2010) Kinetic and fluid dynamics modeling of methane/hydrogen jet flames in diluted coflow. Appl Therm Eng 30:376–383
13. Mardani A, Tabejamaat S, Ghamari M (2010) Numerical study of influence of molecular diffusion in the Mild combustion regime. Combust Theory Model 14(5):747–774
14. Mardani A, Tabejamaat S, Ghamari M (2011) Numerical study of effect of turbulence on rate of reactions in the MILD combustion regime. Combust Theory Model 15(6):753–772
15. Aminian J, Galletti C, Shahhosseini S, Tognotti L (2012) Numerical investigation of a MILD combustion burner: analysis of mixing field, chemical kinetics, and turbulence-chemistry interaction. Flow Turbul Combust 88:597–623
16. Kim SH, Huh KY, Dally BB (2005) Conditional moment closure modeling of turbulent non-premixed combustion in diluted hot coflow. Proc Combust Inst 30:751–757
17. Ihme M, See YC (2011) LES flamelet modeling of three-stream MILD combustor: analysis of flame sensitivity to scalar inflow conditions. Proc Combust Inst 33:1309–1317
18. Ihme M, Zhang J, He G, Dally BB (2012) LES of a Jet-in-Hot-Coflow burner operating in the oxygen-diluted combustion regime. Flow Turbul Combust 89:449–464
19. Kazakov A, Frenklach M (1994) Reduced reaction sets based on GRI-MECH 1.2. http://www.me.berkeley.edu/drm/
20. Bowman CT, Hanson RK, Davidson DF, Gardiner WC Jr, Lissianski V, Smith GP, Golde DM, Frenklach M, Goldenberg M (1999) GRI Mech. http://www.me.berkeley.edu/gri_mech/
21. Bilger RW, Starner SH, Kee RJ (1990) On reduced mechanisms for methane-air combustion in non-premixed flames. Combust Flame 80:135–149
22. Haworth DC (2010) Progress in probability density function methods for turbulent reacting flows. Prog Energy Combust Sci 36:168–259
23. van Oijen JA, Lammers FA, de Goey LPH (2001) Modelling of complex premixed premixed burner systems using flamelet-generated manifolds. Combust Flame 127(3):2124–2134
24. Vreman AW, Albrecht BA, van Oijen JA, de Goey LPH, Bastiaans RJM (2008) Premixed and nonpremixed generated manifolds in large eddy simulation of Sandia flame D and F. Combust Flame 153:394–416
25. Ramaekers WJS, van Oijen JA, de Goey LPH (2010) A priori testing of flamelet generated manifolds for turbulent partially premixed methane/air flames. Flow Turbul Combust 84:439–458
26. Bekdemir C, Somers LMT, de Goey LPH, Tillou J, Angelberger C (2013) Predicting diesel combustion characteristics with large-eddy simulations including tabulated chemical kinetics. Proc Combust Inst 34:3067–3074

27. Sarras G, Mahmoudi Y, Arteaga Mendez LD, van Veen EH, Tummers MJ, Roekaerts DJEM (2014) Modeling of turbulent natural gas and biogas flames of the Delft Jet-in-Hot-Coflow burner: effects of coflow temperature, fuel temperature and fuel composition on the flame lift-off height. Flow Turbul Combust 93(4):607–635
28. CHEM1D. A one-dimensional laminar flame code. Eindhoven University of Technology. https://www.tue.nl/combustion/chem1d
29. an Oijen JA, de Goey LPH (2002) Modelling of premixed counterflow flames using the flamelet-generated manifold method. Combust Thoery Model 6:463–478
30. Peeters TWJ (1995) Numerical modeling of turbulent natural-gas diffusion flames. PhD thesis, Technische Universiteit Delft
31. Naud B, Jiménez C, Roekaerts D (2006) A consistent hybrid PDF method: implementation details and application to the simulation of a bluff-body stabilised flame. Prog Comput Fluid Dyn 6:147–157
32. Naud B, Merci B, Roekaerts D (2010) Generalised Langevin model in correspondence with a chosen standard scalar-flux second-moment closure. Flow Turbul Combust 85:363–382
33. Merci B, Naud B, Roekaerts D (2009) Joint scalar versus joint velocity-scalar PDF simulations of bluff-body stabilized flames with REDIM. Flow Turbul Combust 82(2):185–209
34. Dopazo C, O'Brien EE (1974) Functional formulation of non-isothermal turbulent reactive flows. Phys Fluids 17:1968–7195
35. Curl RL (1963) Dispersed phase mixing: 1. Theory and effects in simple reactors. AIChE J 9:175–181
36. Subramaniam S A mixing model for turbulent reactive flows based on Euclidean minimum spanning trees. Combustion and Flame 115(4):487–514